

Benchmarking Post-Training Quantization of Large Language Models under Microscaling Floating Point Formats

Manyi Zhang* Ji-Fu Li* Zhongao Sun*
 Haoli Bai Hui-Ling Zhen Zhenhua Dong Xianzhi Yu†

Huawei Technologies
 {zhangmanyi6, yuxianzhi}@huawei.com

Abstract

Microscaling Floating-Point (MXFP) has emerged as a promising low-precision format for large language models (LLMs). Despite various post-training quantization (PTQ) algorithms being proposed, they mostly focus on integer quantization, while their applicability and behavior under MXFP formats remain largely unexplored. To address this gap, this work conducts a systematic investigation of PTQ under MXFP formats, encompassing over 7 PTQ algorithms, 15 evaluation benchmarks, and 3 LLM families. The key findings include: 1) MXFP8 consistently achieves near-lossless performance, while MXFP4 introduces substantial accuracy degradation and remains challenging; 2) PTQ effectiveness under MXFP depends strongly on format compatibility, with some algorithmic paradigms being consistently more effective than others; 3) PTQ performance exhibits highly consistent trends across model families and modalities, in particular, quantization sensitivity is dominated by the language model rather than the vision encoder in multi-modal LLMs; 4) The scaling factor of quantization is a critical error source in MXFP4, and a simple pre-scale optimization strategy can significantly mitigate its impact. Together, these results provide practical guidance on adapting existing PTQ methods to MXFP quantization.

1 Introduction

The ever-growing scale of large language models (LLMs) poses a significant deployment challenge due to prohibitive demands for memory and computational resources (Yuan et al., 2024; Dantas et al., 2025). Quantization has therefore emerged as an indispensable technique to mitigate these issues by reducing the numerical precision of weights or activations (Nagel et al., 2021; Kurtic et al., 2025; Huang et al., 2024; Guo et al., 2025; Tang et al.,

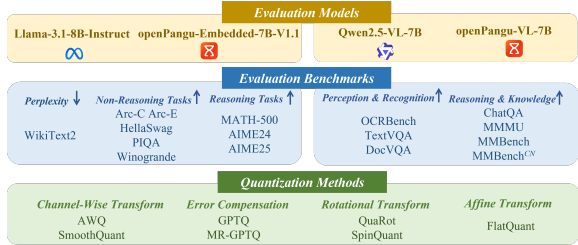


Figure 1: The overview of our empirical evaluations.

2025). Among various low-precision representations, Microscaling Floating-Point (MXFP) formats have attracted increasing attention (Shao et al., 2025). As a block-level number format, MXFP better preserves the dynamic range of full-precision models while benefiting from growing hardware support (Advanced Micro Devices, Inc., 2025; Chouquette, 2023; Tirumala and Wong, 2024).

In this context, post-training quantization (PTQ) provides a practical and training-free route to compress pre-trained models, and a rich line of PTQ techniques has been developed to alleviate the accuracy drop under low precision. However, existing PTQ research and design choices have been predominantly tailored to integer (INT) formats (Frantar et al., 2022; Shao et al., 2023; Ma et al., 2024; Lin et al., 2024a; Dettmers et al., 2022; Li et al., 2024; Wang et al., 2023). This leaves the effectiveness and potentially the distinct failure modes of PTQ on MXFP formats largely underexplored.

In this paper, we provide a comprehensive empirical study of various PTQ methods for MXFP formats, including MXFP8 and MXFP4, as outlined in Figure 1. We systematically categorize existing PTQ methods into four classes: (i) channel-wise transformation, (ii) error compensation, (iii) rotational transformation, and (iv) affine transformation. Our evaluations cover weight-only, weight-activation, and KV cache quantization across multiple bit-width configurations, and span both reasoning and non-reasoning benchmarks. The studied models encompass two different LLM fami-

*Equal contribution. †Corresponding author.

lies (*i.e.*, Llama3.1-8b-Instruct (Grattafiori et al., 2024) and openPangu-Embedded-7B-v1.1 (Chen et al., 2025a)) and multimodal LLMs (MLLM) (*i.e.*, Qwen2.5-VL-7B (Wang et al., 2024) and openPangu-VL-7B (openPangu Team, 2025b)). Based on extensive experiments, we distill several key findings, summarized as follows:

1. **Lossless Quantization** (§3.2): 8-bit weight-activation MXFP quantization is lossless across tasks and modalities. In contrast, 4-bit weight or activation quantization under MXFP results in non-negligible accuracy degradation and remains an open challenge.
2. **Quantization Algorithms** (§3.3): Error compensation and affine transformation methods are more compatible with MXFP quantization, particularly at low bit-widths, and their combination yields stronger performance. Notably, RTN remains a competitive baseline, indicating that MXFP demands quantization methods tailored to its specific scheme.
3. **Impact of Model Family and Modalities** (§3.4): PTQ under MXFP exhibits consistent effectiveness across different model families and modalities. For MLLMs, quantization sensitivity is dominated by the LLM component rather than the vision encoder, favoring mixed-precision designs that preserve higher precision in the LLM. Visual tokens are comparatively robust under MXFP, with reduced bit-width incurring negligible accuracy loss.
4. **Quantization Components** (§3.5): The quantization error introduced by the scaling factors is noticeable. Pre-scale operation, a practically effective optimization strategy for MXFP4, is recommended.

Our empirical study and findings show that MXFP is not merely a drop-in replacement for existing low-precision formats, but also a distinct numerical regime that calls for format-aware quantization design. We hope this work serves as a reference point for future research on MXFP-centric PTQ methods, and encourages the community to move beyond integer-oriented assumptions when developing low-precision algorithms for large-scale foundation models.

2 Preliminary

2.1 Low-Bit Integer (INT) and Floating-Point (FP) Quantization

Quantization maps a tensor \mathbf{W} in high-precision source-format to a lower bit-width, such as low-bit INT and FP formats. For integer quantization, we define:

$$\mathbf{W}_q := \text{clip}([\mathbf{W}/s], Q_{\min}, Q_{\max}) \cdot s, \quad (1)$$

where $\text{clip}([\mathbf{W}/s], Q_{\min}, Q_{\max})$ truncates the associated values inside the minimal Q_{\min} and maximal Q_{\max} , and s is the scaling factor that normalizes \mathbf{W} to the target integer range. More complex than integers, floating-point numbers are encoded using three components (Markstein, 2008): a sign bit (S), an exponent (E), and a mantissa (M). We denote a format as $EaMb$, where a and b are the exponent and mantissa bit numbers. Floating-point quantization is defined as:

$$\mathbf{W}_q := \text{nearest}([\mathbf{W}/s], \mathbb{C}_{\text{FP}}) \cdot s, \quad (2)$$

where \mathbb{C}_{FP} is the set of representable low-bit floating-point values related to S , E , and M (Chen et al., 2025b), and $\text{nearest}(\cdot, \mathbb{C}_{\text{FP}})$ maps normalized values to the nearest element of \mathbb{C}_{FP} .

2.2 Microscaling Floating Point (MXFP) Quantization

The MXFP, proposed by OCP (Rouhani et al., 2023), is a family of quantized floating-point formats that utilize block quantization. An MX-format is specified by the block size 32 and uses a shared UE8M0 data-type for each block. The MXFP8 format has E4M3 and E5M2 variants, and MXFP4 is E2M1. Here, we adopt E4M3 for MXFP8, as a larger mantissa width is more crucial for the performance of fine-grained quantization (Mishra et al., 2025; Chen et al., 2025c).

2.3 Post-training Quantization Methods

We consider quantization under PTQ. Here, we divide PTQ methods into four categories: channel-wise transformation, error compensation, rotational transformation, and affine transformation. For each category, we evaluate representative algorithms that embody its core principle.

Channel-Wise Transformation. Generally, this kind of method aims to reduce quantization error by adaptively adjusting the numerical ranges of activation and weights along individual channels. We

here evaluate two prominent methods, which are SmoothQuant (Xiao et al., 2023) and AWQ (Lin et al., 2024b). SmoothQuant proposes per-channel scaling to migrate quantization difficulty from activations to weights. AWQ is developed to enable efficient quantization of LLMs while preserving the precision of the most critical weights.

Error Compensation. These methods aim to mitigate quantization-induced discrepancies by explicitly modeling and compensating for the quantization error. In this work, we consider GPTQ (Frantar et al., 2022) and MR-GPTQ (Egiazarian et al., 2025). GPTQ performs layer-wise quantization and leverages inverse-Hessian information to update weights, thereby reducing accuracy degradation. MR-GPTQ extends GPTQ to better match the characteristics of FP4 quantization by incorporating block-wise Hadamard transforms and format-specific optimizations.

Rotational Transformation. This class of methods utilizes pre-quantized orthogonal transformations to the weight and activations. These transformations can reconstruct the data distribution to mitigate the impact of extreme outliers on activations. We assess QuaRot (Ashkboos et al., 2024), which uses random orthogonal rotations, and Spin-Quant (Liu et al., 2024c), which employs learnable rotations optimized during calibration.

Affine Transformation. These methods improve low-bit model compression by applying learnable, rescaling transformations to weights and activations before quantization, explicitly redistributing numerical magnitudes across dimensions. We include FlatQuant (Sun et al., 2024). To achieve flatter distributions of weights and activations, FlatQuant identifies layer-wise optimal affine transformations by employing a lightweight, block-wise training strategy over the calibration stage.

3 Evaluations

3.1 Setup

Quantization Settings. We study several MXFP-based quantization configurations. (1) *Weight-Only Quantization*. Only the weight tensors of linear layers are quantized using MXFP formats, while activations remain in full precision. (2) *Weight-Activation Quantization*. Weights and input activation tensors are quantized using MXFP, enabling fully quantized matmul operations. (3) *KV*

Cache Quantization. The key and value tensors in attention blocks are quantized to reduce the memory footprint during inference. For clarity, we denote each configuration using the format $W\{bits\}A\{bits\}[KV\{bits\}]$. For example, W4A8 indicates quantizing weights to 4-bit and activations to 8-bit.

Evaluation Benchmarks. We assess quantized models on the following benchmarks. (1) Language modeling quality via perplexity (PPL) on WikiText2 (Merity et al., 2016). (2) Non-reasoning tasks (zero-shot), including PIQA (Bisk et al., 2020), Winogrande (Sakaguchi et al., 2021), Hellaswag (Zellers et al., 2019), ARC-Easy (Clark et al., 2018), and ARC-Challenge (Clark et al., 2018). (3) Reasoning benchmarks, such as MATH-500 (Lightman et al., 2023), AIME24 and AIME25. (4) Multimodal benchmarks, including OCRBench (Liu et al., 2024b), MM-Bench (Liu et al., 2024a), MMBench^{CN} (Zhang et al., 2025), TextVQA (Singh et al., 2019), ChartQA (Masry et al., 2022), MME (Fu et al., 2025), and MMMU (Yue et al., 2024). To simulate the quantization with MXFP format, we use the microxcalng library¹ for all experiments. Details of the evaluation are provided in Appendix A.1.

Evaluation Models. We evaluate two popular LLMs, including Llama-3.1-8B-Instruct (Grattafiori et al., 2024) and openPangu-Embedded-7B-V1.1 (Chen et al., 2025a). Llama-3.1-8B-Instruct is an instruction-tuned LLM based on the Llama-3 architecture, offering strong multilingual and reasoning capabilities. openPangu-Embedded-7B-V1.1 is an efficient reasoning-focused LLM featuring a dual-system (fast/slow) inference capability. To further investigate the performance of MXFP quantization on the MLLM, we additionally evaluate the Qwen2.5-VL-7B (Wang et al., 2024) and openPangu-VL-7B models (openPangu Team, 2025b).

We explore the following questions in the subsequent sections.

¹<https://github.com/microsoft/microxcalng>

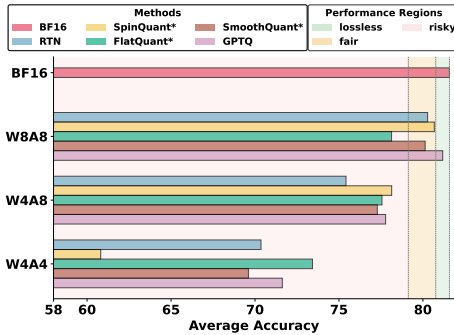


Figure 2: Average accuracy of Reasoning tasks on openPangu-Embedded-7B-V1.1.

RQ1 (§3.2): What is the impact of different MXFP formats on model accuracy?

RQ2 (§3.3): How do various post-training quantization methods perform with MXFP?

RQ3 (§3.4): How do different model families and modalities affect quantization?

RQ4 (§3.5): How do quantization design choices impact MXFP4 performance?

3.2 Performance on Different MXFP Quantization Settings (RQ1)

Following prior work (Liu et al., 2025), we categorize post-quantization performance degradation into three regimes based on average accuracy recovery rate relative to BF16: **lossless** ($\leq 1\%$), **fair** ($1\%-3\%$), and **risky** ($\geq 3\%$). The overall results achieved by Llama-3.1-8B-Instruct, openPangu-Embedded-7B-V1.1, and Qwen2.5-VL-7B are summarized in Tables 1, 2, and 3. We also provide the results of reasoning tasks in Figure 2 (details in Appendix A.2.1). Note that the results across W8A8, W4A8, and W4A4 settings reveal a clear spectrum of quantization difficulty, which is largely dictated by the bit width of weights and activations. Below, we discuss these results.

W8A8 is generally safe for deployment. According to Tables 1, 2, and 3, the majority of PTQ methods consistently achieve lossless performance regardless of their internal design. This suggests that 8-bit quantization of both weights and activations is largely benign for modern LLMs and MLLMs, and can be safely deployed without extensive calibration or architectural adaptation.

W4A8 should be approached with caution. We find that the transition to W4A8 with RTN incurs noticeable accuracy degradation, marking a critical inflection point. However, with PTQ algorithms, performance loss can be mitigated. As seen in Table 2, the accuracy recovery rate is improved from 95.44% to 98.60% after optimization on openPangu-Embedded-7B-V1.1 and achieves near-lossless on Llama-3.1-8B-Instruct. On reasoning tasks, the accuracy improves significantly, but still falls into the risky region. These results indicate that while 4-bit weights challenge the model’s representational capacity, algorithmic refinements can enable W4A8 to be more viable, especially for non-reasoning tasks.

W4A4 is highly risky. The most challenging setting is W4A4, where weights and activations are aggressively quantized. Performance degradation becomes more severe and widespread: accuracy recovery rate falls to 87.25%–96.79%, 86.37%–95.28%, and 92.72%–97.36% for Llama-3.1-8B-Instruct, openPangu-Embedded-7B-V1.1, and Qwen2.5-VL-7B, respectively, entering the risky regime for nearly all methods. Interestingly, the performance gap across different PTQ methods is markedly amplified under this extreme compression. This suggests that when quantization noise exceeds a critical threshold, differences in how methods handle outlier distributions, dynamic range alignment, or activation sensitivity become decisive.

Takeaways 1

W8A8 is consistently lossless across models and benchmarks, and is robust to the choice of PTQ methods. Bridging the performance gap for 4-bit weight or activation quantization (*cf.*, W4A8 and W4A4) under MXFP remains an open challenge.

3.3 Comparison of PTQ Methods (RQ2)

We evaluate diverse PTQ methods under MXFP (see the method descriptions in Section 2.3). The main paper covers bit-width configurations of W8A8, W4A8, and W4A4, as shown in Tables 1, 2, and 3. Results on openPangu-VL-7B and more bit-width configurations (including W4A16 and W4A8KV8) can be found in Appendix A.2.2 and A.2.3, respectively. Below, we summarize these results.

Error compensation methods outperform channel-wise transformations in most scenarios.

Bits	Method	ACC (0-shot) \uparrow							PPL \downarrow
		ARC-C	ARC-E	HellaSwag	PIQA	Winogrande	Avg.	Recovery (%)	
BF16	-	55.20	79.63	79.15	81.07	73.95	73.80	100.00	7.21
W8A8	RTN	53.50	78.45	79.11	80.14	73.64	72.97	98.87	7.31
	QuaRot	55.72	80.09	78.76	80.58	73.64	73.76	99.94	7.39
	QuaRot*	56.4	80.81	78.84	81.01	74.35	74.28	100.65	7.40
	SpinQuant	55.89	80.18	78.60	80.79	74.51	73.99	100.26	7.39
	SpinQuant*	54.35	80.09	78.12	80.2	73.8	73.31	99.34	7.41
	FlatQuant	55.80	79.46	78.99	81.12	73.80	73.83	100.05	7.27
	FlatQuant*	54.69	79.42	78.56	80.63	74.19	73.50	99.59	7.33
	AWQ	54.27	79.17	78.48	80.74	73.80	73.29	99.31	7.34
	SmoothQuant	55.38	79.08	79.14	81.23	74.51	73.87	100.09	7.34
	SmoothQuant*	55.03	79.63	78.73	81.39	73.88	73.73	99.91	7.34
W4A8	MR-GPTQ	55.38	79.12	78.99	81.01	73.95	73.69	99.85	7.24
	GPTQ	54.69	79.12	78.47	80.79	74.35	73.48	99.57	7.33
	RTN	53.07	76.81	77.04	80.03	73.48	72.09	97.68	7.71
	QuaRot	49.15	75.93	76.37	78.29	71.03	70.15	95.06	8.45
	QuaRot*	52.65	79.67	77.86	80.52	73.40	72.82	98.67	7.95
	SpinQuant	49.91	75.59	76.10	78.07	71.90	70.31	95.28	8.50
	SpinQuant*	52.82	78.37	76.96	79.6	73.32	72.21	97.85	7.84
	FlatQuant	53.84	80.26	77.27	80.03	71.82	72.64	98.43	7.87
	FlatQuant*	53.84	80.26	77.27	80.03	71.82	72.64	97.95	7.81
	AWQ	53.84	79.25	77.55	79.98	73.88	72.90	98.78	7.75
W4A4	SmoothQuant	54.01	77.61	77.77	79.98	74.98	72.87	98.74	7.75
	SmoothQuant*	52.96	77.02	77.42	78.63	70.64	71.33	96.67	8.70
	MR-GPTQ	54.52	78.62	77.28	80.47	73.80	72.94	98.83	7.83
	GPTQ	53.5	79.59	79.71	81.18	73.6	73.52	99.62	7.87
	RTN	49.66	75.80	75.48	79.05	70.48	70.09	94.98	8.27
	QuaRot	44.11	71.63	71.82	75.14	64.88	65.52	88.78	10.34
	QuaRot*	49.15	74.62	74.26	77.48	68.98	68.90	93.36	9.12
	SpinQuant	43.09	67.26	70.71	74.92	65.98	64.39	87.25	10.40
	SpinQuant*	49.15	74.54	74.38	76.99	69.53	68.92	93.38	9.01
	FlatQuant	52.05	77.27	76.89	79.49	70.64	71.27	96.57	8.03
	FlatQuant*	51.19	78.58	76.77	78.94	71.67	71.43	96.79	8.06
	AWQ	52.30	77.95	76.13	78.92	69.46	70.95	96.14	8.25
	SmoothQuant	51.37	76.52	76.12	79.00	72.38	71.08	96.31	8.25
	SmoothQuant*	50.51	73.36	75.27	76.82	67.17	68.63	92.98	8.50
	MR-GPTQ	50.85	75.46	76.02	79.82	70.80	70.59	95.65	8.34
	GPTQ	50.68	77.65	75.66	78.18	70.24	70.48	95.50	8.37

Table 1: Comparison of PTQ methods on **Llama-3.1-8B-Instruct** under W8A8, W4A8, and W4A4 in terms of **non-reasoning** downstream task accuracy and perplexity. * denotes the variant integrated with the GPTQ algorithm.

We observe that error compensation methods (*e.g.*, GPTQ and MR-GPTQ) consistently outperform channel-wise transformation methods (*e.g.*, SmoothQuant and AWQ), except in the case of Llama-3.1-8B-Instruct under W4A4. For example, based on Table 2, under W4A8, error compensation methods recover 97.03%–97.36% of BF16 performance, outperforming channel-wise transformations (96.25%–96.33%). This performance gap may stem from the following: channel-wise scaling operates at a coarser granularity and cannot fully capture intra-group magnitude variations under MXFP’s group-wise quantization. Although error compensation methods like GPTQ also operate primarily at the channel level, they explicitly minimize quantization error during calibration, thereby providing a stronger guarantee.

Rotational transformation impairs MXFP4 quantization. Unlike remarkable success in INT4 formats, Rotation-based methods (*e.g.*, QuaRot, SpinQuant) consistently degrade MXFP4 quantization accuracy, performing worse than the RTN baseline. Specifically, Table 1 shows that

RTN achieves a lower perplexity (8.27) compared to QuaRot (10.34) and SpinQuant (10.40) under W4A4. On non-reasoning benchmarks, QuaRot and SpinQuant exhibit relative recovery rate degradations of 6.20% and 7.73% compared to RTN, respectively. The harm likely stems from the fact that MXFP4 uses group-wise scaling and relies on local statistical properties (*e.g.*, distribution shape within each group) to preserve information during quantization. Global rotations mix information across all dimensions, flattening outlier structures and reducing kurtosis, which makes the distribution less amenable to effective group-wise scaling.

Affine transformation is most robust under 4-bit quantization. Across all LLMs, affine transformation (*i.e.*, FlatQuant) exhibits the most robust performance under W4A4. For example, on Llama-3.1-8B-Instruct (see Table 1), FlatQuant attains an accuracy recovery rate of 96.57%, clearly surpassing RTN (94.98%), SpinQuant (87.25%), and even the strong error compensation method MR-GPTQ (95.65%), while also achieving the lowest WikiText perplexity (8.03). The difference likely arises from

Bits	Method	ACC (0-shot) \uparrow							PPL \downarrow
		ARC-C	ARC-E	HellaSwag	PIQA	Winogrande	Arg.	Recovery. (%)	
BF16	-	42.75	67.26	62.86	73.50	60.62	61.40	100.00	34.89
W8A8	RTN	44.03	66.25	61.74	73.61	57.77	60.68	98.83	35.75
	QuaRot	42.24	65.95	62.45	72.42	60.69	60.75	98.94	35.21
	QuaRot*	42.83	68.22	62.18	73.78	60.96	61.59	100.32	35.75
	SpinQuant	42.49	67.34	62.42	72.31	60.30	60.97	99.31	35.49
	SpinQuant*	42.58	68.43	62.52	73.94	59.59	61.41	100.02	33.04
	FlatQuant	43.43	68.64	62.25	73.78	59.04	61.43	100.05	30.96
	FlatQuant*	43.86	69.23	62.33	74.05	61.33	62.16	101.24	30.87
	AWQ	41.98	68.48	61.16	72.58	61.09	61.06	99.45	38.00
	SmoothQuant	42.58	66.50	62.08	72.69	59.19	60.61	98.71	35.25
	SmoothQuant*	42.15	66.67	61.84	72.36	59.59	60.52	98.57	35.00
W4A8	MR-GPTQ	43.09	67.80	62.84	73.72	59.91	61.47	100.12	34.57
	GPTQ	42.92	67.13	61.66	72.69	57.85	60.45	98.46	34.75
	RTN	39.59	65.24	58.70	71.60	57.85	58.60	95.44	42.17
	QuaRot	40.10	64.10	57.95	72.69	57.70	58.51	95.29	40.87
	QuaRot*	40.02	65.07	58.54	71.44	57.62	58.54	95.84	43.83
	SpinQuant	39.59	61.57	58.56	72.09	58.17	58.00	94.46	38.94
	SpinQuant*	42.41	67.85	60.74	72.91	58.8	60.54	98.60	34.75
	FlatQuant	40.78	66.54	60.15	72.52	58.17	59.63	97.12	37.67
	FlatQuant*	42.15	67.63	60.54	72.80	57.38	60.10	97.89	37.72
	AWQ	39.85	66.25	58.13	73.07	58.17	59.09	96.25	41.75
W4A4	SmoothQuant	40.78	66.20	58.82	72.47	57.46	59.15	96.33	43.25
	SmoothQuant*	41.64	67.47	59.88	73.07	58.88	60.19	98.03	40.00
	MR-GPTQ	40.87	66.84	60.64	72.63	57.93	59.78	97.36	39.19
	GPTQ	40.96	65.51	59.48	72.42	59.51	59.58	97.03	37.50
	RTN	38.48	61.53	56.42	70.46	56.91	56.76	92.45	49.33
	QuaRot	36.43	56.19	51.24	66.76	54.54	53.03	86.37	56.19
	QuaRot*	36.09	59.30	53.06	68.55	55.33	54.47	88.71	53.75
	SpinQuant	34.64	57.24	52.82	68.39	55.49	53.72	87.49	51.09
	SpinQuant*	37.88	60.4	55.34	69.53	57.22	56.07	91.33	46.28
	FlatQuant	39.93	65.82	57.07	71.00	56.04	57.97	94.42	38.36
W4A4	FlatQuant*	40.19	66.84	58.13	69.80	57.54	58.50	95.28	36.40
	AWQ	37.08	63.76	54.49	71.06	57.70	56.82	92.54	46.00
	SmoothQuant	38.99	65.07	55.81	70.80	56.70	57.47	93.60	52.00
	SmoothQuant*	38.65	64.60	56.74	70.73	57.62	57.67	93.92	43.57
	MR-GPTQ	38.99	63.43	57.19	69.48	58.96	57.61	93.83	42.17
	GPTQ	39.25	62.75	57.47	69.91	56.99	57.27	93.28	44.50

Table 2: Comparison of PTQ methods on **openPangu-Embedded-7B-V1.1** under W8A8, W4A8, and W4A4 about **non-reasoning** downstream task accuracy and perplexity. * denotes the variant integrated with the GPTQ algorithm.

the fact that, whereas orthogonal rotations preserve the L_2 norm, FlatQuant employs learnable affine transformations that do not conserve total energy. Although the global affine transforms of FlatQuant may still propagate energy across groups, their ability to modulate absolute magnitudes makes them better suited for low-bit MXFP quantization. To better understand how these methods reshape activation distributions, we visualize activation distributions under W4A4 in Figure 5. As illustrated in the figure, different quantization strategies induce markedly distinct activation distributions. Rotation-based approaches still preserve a relatively large activation magnitude compared to FlatQuant.

RTN remains a strong baseline across all bit-widths. The experimental phenomenon underscores a critical limitation: most existing PTQ methods were designed and optimized for the INT format. However, these methods frequently fail to align with the quantization scheme of the MXFP format, yielding only marginal gains, or even re-

gressions, over RTN when naively transferred to MXFP. This suggests that effective quantization methods for the MXFP format require designs that explicitly account for its quantization scheme.

Takeaways 2

Error compensation and affine transformations are better aligned with MXFP quantization, especially at low bit-widths. The persistence of RTN as a strong baseline suggests that MXFP requires quantization methods designed for its specific scheme.

3.4 Impact of Model Families and Modalities (RQ3)

To assess how quantization performance varies across model families and modalities, we evaluate models along two dimensions: (i) models with different modalities (*i.e.*, Llama-3.1-8B-Instruct vs. Qwen2.5-VL-7B), and (ii) models of the same modality but from different families (*i.e.*, Llama-3.1-8B-Instruct vs. openPangu-Embedded-7B-V1.1).

Bits	Method	OCR Bench	MMBench	MMBench ^{CN}	TextVQA	ChartQA	MME	MMMU	Recovery (%)
BF16	—	877	79.08	75.95	84.61	85.61	2321	49.5	100.00
W8A8	RTN	879	78.32	75.34	84.32	86.68	2312	50.1	100.03
	QuaRot	874	79.00	75.86	84.21	86.20	2302	49.9	99.95
	QuaRot*	873	78.32	74.48	83.90	86.60	2300	49.2	99.35
	SpinQuant	880	78.66	74.74	84.33	86.32	2323	48.6	99.57
	SpinQuant*	881	79.12	75.16	84.63	86.42	2325	49.4	100.06
	FlatQuant	879	79.17	75.95	84.63	86.64	2329	50.2	100.48
	FlatQuant*	878	78.66	75.69	84.51	86.28	2339	50.3	100.33
	AWQ	873	78.15	76.03	83.46	86.16	2300	49.9	99.67
	SmoothQuant	874	78.32	75.09	83.73	86.28	2337	49.2	99.63
W4A8	SmoothQuant*	883	78.49	76.37	83.75	85.40	2314	50.3	100.08
	GPTQ	872	78.49	76.29	84.29	85.81	2315	50.2	100.02
	RTN	855	78.57	76.80	82.74	84.56	2240	50.3	98.95
	QuaRot	863	77.98	73.63	82.87	85.08	2297	49.1	98.49
	QuaRot*	859	79.00	76.55	82.91	84.60	2208	49.2	98.57
	SpinQuant	864	77.89	74.40	83.30	85.68	2137	49.6	97.97
	SpinQuant*	866	78.40	73.97	83.81	85.72	2271	50.9	99.31
	FlatQuant	861	76.70	75.77	81.81	86.28	2287	49.2	98.62
	FlatQuant*	870	76.87	73.59	82.96	86.28	2307	49.5	98.79
W4A4	AWQ	866	77.72	74.31	81.82	85.48	2314	48.5	98.44
	SmoothQuant	849	76.19	74.44	81.1	84.36	2242	47.6	96.90
	SmoothQuant*	868	78.32	75.43	83.45	85.08	2275	48.7	98.82
	GPTQ	864	77.89	76.03	83.18	85.80	2325	50.2	99.61
	RTN	845	77.04	74.88	78.62	82.97	2194	46.1	95.69
	QuaRot	843	73.83	68.73	78.89	81.76	2195	46.3	93.83
	QuaRot*	840	75.34	71.91	80.20	84.56	2103	47.0	94.98
	SpinQuant	843	73.21	69.17	78.98	80.76	2006	47.1	92.72
	SpinQuant*	851	74.83	70.19	80.29	82.60	2190	47.2	95.02
W4A4	FlatQuant	853	75.26	74.31	80.14	85.44	2293	47.2	96.99
	FlatQuant*	860	74.23	69.67	81.56	86.32	2287	48.4	96.74
	AWQ	840	74.83	72.08	79.71	83.32	2249	47.3	95.61
	SmoothQuant	843	75.26	72.51	81.26	84.04	2204	49.6	96.59
	SmoothQuant*	843	76.62	73.20	81.35	84.60	2231	47.0	96.49
	GPTQ	846	76.19	73.97	81.12	83.72	2336	48.0	97.36

Table 3: Comparison of PTQ methods on **Qwen2.5-VL-7B** under W8A8, W4A8, and W4A4 quantization across multimodal benchmarks. * denotes the variant integrated with the GPTQ algorithm.

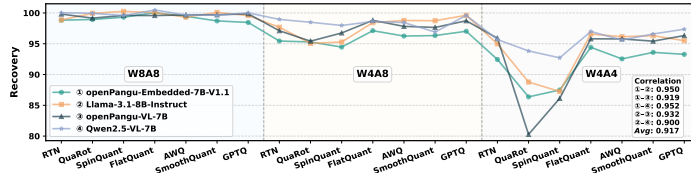


Figure 3: Recovery rate performance of various PTQ methods across MXFP quantization settings. Each curve represents results from all quantization settings of a model. We also show the pairwise correlation of two different models. The correlation is calculated using the Pearson correlation coefficient (Benesty et al., 2009)) among their performance curves and observe a high degree of consistency, with an average pairwise correlation of 0.917. This strong alignment indicates that PTQ methods under MXFP exhibit similar performance trends across architectures and modalities, suggesting that their effectiveness is not strongly model- or modality-dependent.

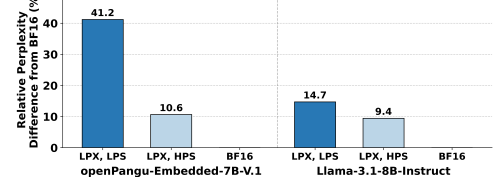


Figure 4: Impact of scaling factor error. Restoring low-precision values and low-precision scales (LPX, LPS) to low-precision values with high-precision scales (LPX, HPS) leads to a clear reduction in perplexity (PPL).

LLM	ViT	OCRBench	MMBench	MMBench ^{CN}	TextVQA	ChartQA	MME	MMMU	Recovery (%)
W8A8	W4A4	856	77.08	75.95	84.61	85.56	2288	49.3	98.96
	W8A8	879	78.32	75.34	84.32	86.68	2312	50.1	100.03
	W4A4	845	77.04	74.88	78.62	82.97	2194	46.1	95.69

Table 4: Comparison of the impact of the LLM and ViT quantization under RTN on Qwen-2.5-VL-7B. Recovery (%) is computed relative to the BF16 baseline.

In MLLMs, quantization sensitivity is dominated by the LLM rather than vision Transformer. To dissect the contribution of each component of MLLMs to final results, we separately quantize the LLM and vision Transformer (ViT) in Qwen2.5-VL-7B using RTN. As seen in Table 4, reducing the LLM from W8A8 to W4A4 induces a significant accuracy recovery rate drop

LLM Weights	Textual	Visual	OCR	CRBench	MMBench	MMBench ^{CN}	TextVQA	ChartQA	MME	MMMU	Recovery (%)
W16	A16	A16		918	85.46	85.40	83.92	87.68	2287	54.5	100.00
	A16	A16		902	85.37	85.14	85.00	88.00	2302	53.5	99.45
	A4	A16		902	84.35	84.45	83.68	87.32	2335	54.4	99.32
	A4	A4		908	83.59	82.13	83.42	87.36	2289	51.5	98.07
W4	A8	A8		888	83.42	83.16	82.56	86.44	2270	53.2	97.89
	A8	A4		878	82.91	83.16	82.26	86.52	2223	51.6	96.95
	A4	A8		873	82.48	82.39	81.87	86.04	2268	51.4	96.75
	A4	A4		873	82.48	82.56	81.39	86.00	2259	50.7	96.45
W4*	A8	A8		899	85.29	83.85	83.4	87.28	2295	53.0	98.92
	A8	A4		886	84.87	84.16	83.2	87.44	2316	53.6	98.98
	A4	A8		893	83.59	82.56	82.9	86.92	2288	51.9	97.85
	A4	A4		876	82.91	81.96	83.06	86.88	2280	52.8	97.58

Table 5: Comparison of activation quantization for textual and visual tokens under different settings in openPangu-VL-7B. Weights are kept in full precision (W16) or quantized to 4-bit (W4) using RTN; the * indicates GPTQ-based weight quantization. Note that the ViT component remains unquantized.

(3% in Qwen2.5-VL-7B), whereas applying the same W4A4 quantization to the ViT results in approximately 1% degradation. These results suggest a practical and effective quantization policy: retain higher precision (*e.g.*, W8A8) in the LLM while aggressively quantizing the ViT (*e.g.*, W4A4). Under this configuration, the model achieves nearly lossless accuracy while reducing memory footprint and the latency of the first token generation, making it a compelling default for realistic multimodal deployments.

Visual tokens are more robust under MXFP quantization compared to INT formats. Prior studies have shown that quantizing MLLMs to INT formats is particularly challenging, as visual tokens exhibit significantly larger outliers and a wider activation range than their textual counterparts (Yu et al., 2025; Xue et al., 2025). However, as shown in Table 5, under MXFP quantization, reducing the bit-width allocated to visual tokens does not result in noticeable accuracy degradation. This observation may be associated with MXFP’s exponent–mantissa decoupling, which allows more flexible handling of wide activation ranges while maintaining enough precision.

Takeaways 3

PTQ methods under MXFP exhibit consistent effectiveness across models and modalities. In MLLMs, quantization sensitivity is dominated by the LLM rather than the ViT, favoring a mixed-precision design that preserves higher LLM precision. Visual tokens are more robust under MXFP than INT, with reduced bit-width causing no noticeable accuracy loss.

3.5 Analysis of MXFP4 Quantization Components (RQ4)

Quantization Error From Scaling Factors. Considering the non-trivial quantization error intro-

Strategy	Metric						
	ARC-C	ARC-E	HellaSwag	PIQA	Winogrande	Avg Acc ↑	PPL ↓
✓	38.48	61.53	56.42	70.46	56.91	56.76	49.33
✗	32.34	58.12	48.76	67.41	55.33	52.39	104.42

Table 6: Ablation study of optimization strategy for openPangu-Embedded-7B-V1.1 under W4A4. *Pre-scale* refers to scaling inputs before computing quantization parameters.

duced by MXFP4 quantization, we study the error introduced by the scaling factors. FP8 block-level scaling factors s in MXFP formats must satisfy the constraints of the E8M0 data type. Following (Cook et al., 2025), we keep the scaling factors in high precision while still mapping the scaled values onto the FP4 representable grid, and compute the relative perplexity (PPL) difference from BF16, as shown in Figure 4. We observe that errors from scaling factors have a significant impact on model performance. When the error of scaling factors is addressed, the relative perplexity (PPL) improves clearly. This impact stems from the E8M0 format, which forces scaling factors to be powers of two. This coarse quantization often results in a large mismatch between the optimal scale and the allowed scale, thereby affecting all values in its block.

Pre-Scale Strategy. As pointed out in (Tseng et al., 2025), we adopt the unbiased MXFP4 quantization strategy to mitigate systematic clipping bias introduced by the limited FP4 dynamic range. Specifically, the input is first scaled by a factor of 3/4 before quantization, effectively preventing clipping while preserving relative magnitudes. As shown in Table 6, enabling *Pre-scale* operation enhances performance from 52.39% to 56.76% and reduces PPL from 104.42 to 49.33.

Takeaways 4

The quantization error from scaling factors is not negligible. The *Pre-scale* optimization strategy is recommended.

4 Conclusion

This work systematically studies PTQ under MXFP formats. We show that MXFP8 supports stable, near-lossless deployment. Quantization effectiveness under MXFP is governed by compatibility with its block floating-point scheme, resulting in consistent performance differences across algorithmic paradigms. Across model families and modalities, PTQ performance exhibits highly aligned

trends. In multimodal models, quantization sensitivity is dominated by the language component. We further identify scaling-factor quantization as a key error source in MXFP4 and show that a simple pre-scale optimization strategy can effectively mitigate its impact. Overall, MXFP should be treated as a distinct numerical regime rather than a drop-in replacement for integer formats. Our findings provide practical guidance for MXFP-aware quantization design.

Limitation

Our study is conducted on 7B/8B-scale LLMs and MLLMs and focuses on MXFP formats. While these settings cover widely used foundation models and representative microscaling designs, we do not evaluate substantially larger models (*e.g.*, 30B-scale models) or NVIDIA-specific NVFP formats (*e.g.*, NVFP4 and NVFP8). Although many observations appear to arise from intrinsic properties of block floating-point quantization and therefore suggest a degree of generality, it remains unclear how well these conclusions extend to much larger model scales or to alternative microscaling formats with different exponent and scaling designs. A systematic investigation along these directions is left for future work.

References

Advanced Micro Devices, Inc. 2025. [AMD CDNA™ 4 Architecture Whitepaper](#). White paper, Advanced Micro Devices, Inc. Accessed: 2025-09-24.

Saleh Ashkboos, Amirkeivan Mohtashami, Maximilian L Croci, Bo Li, Pashmina Cameron, Martin Jaggi, Dan Alistarh, Torsten Hoefer, and James Hensman. 2024. Quarot: Outlier-free 4-bit inference in rotated llms. In [NeurIPS](#), pages 100213–100240.

Jacob Benesty, Jingdong Chen, Yiteng Huang, and Israel Cohen. 2009. Pearson correlation coefficient. In [Noise Reduction in Speech Processing](#), pages 1–4.

Yonatan Bisk, Rowan Zellers, Jianfeng Gao, Yejin Choi, and 1 others. 2020. Piqa: Reasoning about physical commonsense in natural language. In [AAAI](#), volume 34, pages 7432–7439.

Hanting Chen, Yasheng Wang, Kai Han, Dong Li, Lin Li, Zhenni Bi, Jinpeng Li, Haoyu Wang, Fei Mi, Mingjian Zhu, and 1 others. 2025a. Pangu embedded: An efficient dual-system llm reasoner with metacognition. [arXiv preprint arXiv:2505.22375](#).

Mengzhao Chen, Meng Wu, Hui Jin, Zhihang Yuan, Jing Liu, Chaoyi Zhang, Yunshui Li, Jie Huang, Jin Ma, Zeyue Xue, and 1 others. 2025b. Int vs fp: A comprehensive study of fine-grained low-bit quantization formats. [arXiv preprint arXiv:2510.25602](#).

Yuxiang Chen, Haocheng Xi, Jun Zhu, and Jianfei Chen. 2025c. Oscillation-reduced mxfp4 training for vision transformers. [arXiv preprint arXiv:2502.20853](#).

Jack Choquette. 2023. Nvidia hopper h100 gpu: Scaling performance. [IEEE Micro](#), 43(3):9–17.

Peter Clark, Isaac Cowhey, Oren Etzioni, Tushar Khot, Ashish Sabharwal, Carissa Schoenick, and Oyvind Tafjord. 2018. Think you have solved question answering? try arc, the ai2 reasoning challenge. [arXiv preprint arXiv:1803.05457](#).

Jack Cook, Junxian Guo, Guangxuan Xiao, Yujun Lin, and Song Han. 2025. Four over six: More accurate nvfp4 quantization with adaptive block scaling. [arXiv preprint arXiv:2512.02010](#).

Pierre V Dantas, Lucas C Cordeiro, and Waldir SS Júnior. 2025. A review of state-of-the-art techniques for large language model compression. [Complex & Intelligent Systems](#), 11(9):407.

Tim Dettmers, Mike Lewis, Younes Belkada, and Luke Zettlemoyer. 2022. Gpt3. int8 (): 8-bit matrix multiplication for transformers at scale. In [NeurIPS](#), volume 35, pages 30318–30332.

Vage Egiazarian, Roberto L Castro, Denis Kuznedelev, Andrei Panferov, Eldar Kurtic, Shubhra Pandit, Alexandre Marques, Mark Kurtz, Saleh Ashkboos, Torsten Hoefer, and 1 others. 2025. Bridging the gap between promise and performance for microscaling fp4 quantization. [arXiv preprint arXiv:2509.23202](#).

Elias Frantar, Saleh Ashkboos, Torsten Hoefer, and Dan Alistarh. 2022. Gptq: Accurate post-training quantization for generative pre-trained transformers. [arXiv preprint arXiv:2210.17323](#).

Chaoyou Fu, Peixian Chen, Yunhang Shen, Yulei Qin, Mengdan Zhang, Xu Lin, Jinrui Yang, Xiawu Zheng, Ke Li, Xing Sun, and 1 others. 2025. Mme: A comprehensive evaluation benchmark for multimodal large language models. In [NeurIPS Datasets and Benchmarks Track](#).

Leo Gao, Jonathan Tow, Baber Abbasi, Stella Biderman, Sid Black, Anthony DiPofi, Charles Foster, Laurence Golding, Jeffrey Hsu, Alain Le Noac'h, Haonan Li, Kyle McDonell, Niklas Muennighoff, Chris Ociepa, Jason Phang, Laria Reynolds, Hailey Schoelkopf, Aviya Skowron, Lintang Sutawika, and 5 others. 2024. The language model evaluation harness.

Aaron Grattafiori, Abhimanyu Dubey, Abhinav Jauhri, Abhinav Pandey, Abhishek Kadian, Ahmad Al-Dahle, Aiesha Letman, Akhil Mathur, Alan Schelten, Alex Vaughan, and 1 others. 2024. The llama 3 herd of models. [arXiv preprint arXiv:2407.21783](#).

Daya Guo, Dejian Yang, Haowei Zhang, Junxiao Song, Ruoyu Zhang, Runxin Xu, Qihao Zhu, Shiron Ma, Peiyi Wang, Xiao Bi, and 1 others. 2025. Deepseek-r1: Incentivizing reasoning capability in llms via reinforcement learning. [arXiv preprint arXiv:2501.12948](#).

Nathan Habib, Clémentine Fourrier, Hynek Kydlíček, Thomas Wolf, and Lewis Tunstall. 2023. Lighteval: A lightweight framework for llm evaluation.

Wei Huang, Xudong Ma, Haotong Qin, Xingyu Zheng, Chengtao Lv, Hong Chen, Jie Luo, Xiaojuan Qi, Xianglong Liu, and Michele Magno. 2024. How good are low-bit quantized llama3 models? an empirical study. [CoRR](#).

Eldar Kurtic, Alexandre Noll Marques, Shubhra Pandit, Mark Kurtz, and Dan Alistarh. 2025. “give me bf16 or give me death”? accuracy-performance trade-offs in llm quantization. In [ACL](#), pages 26872–26886.

Woosuk Kwon, Zhuohan Li, Siyuan Zhuang, Ying Sheng, Lianmin Zheng, Cody Hao Yu, Joseph Gonzalez, Hao Zhang, and Ion Stoica. 2023. Efficient memory management for large language model serving with pagedattention. In [SOSP](#), pages 611–626.

Muyang Li, Yujun Lin, Zhekai Zhang, Tianle Cai, Xiuyu Li, Junxian Guo, Enze Xie, Chenlin Meng, Jun-Yan Zhu, and Song Han. 2024. Svdquant: Absorbing outliers by low-rank components for 4-bit diffusion models. [arXiv preprint arXiv:2411.05007](#).

Hunter Lightman, Vineet Kosaraju, Yuri Burda, Harrison Edwards, Bowen Baker, Teddy Lee, Jan Leike, John Schulman, Ilya Sutskever, and Karl Cobbe. 2023. Let’s verify step by step. In [ICLR](#).

Haokun Lin, Haobo Xu, Yichen Wu, Jingzhi Cui, Yingtao Zhang, Linzhan Mou, Linqi Song, Zhenan Sun, and Ying Wei. 2024a. Duquant: Distributing outliers via dual transformation makes stronger quantized llms. In [NeurIPS](#), pages 87766–87800.

Ji Lin, Jiaming Tang, Haotian Tang, Shang Yang, Wei-Ming Chen, Wei-Chen Wang, Guangxuan Xiao, Xingyu Dang, Chuang Gan, and Song Han. 2024b. Awq: Activation-aware weight quantization for on-device llm compression and acceleration. [Proceedings of Machine Learning and Systems](#), 6:87–100.

Ruikang Liu, Yuxuan Sun, Manyi Zhang, Haoli Bai, Xianzhi Yu, Tiezheng Yu, Chun Yuan, and Lu Hou. 2025. Quantization hurts reasoning? an empirical study on quantized reasoning models. [arXiv preprint arXiv:2504.04823](#).

Yuan Liu, Haodong Duan, Yuanhan Zhang, Bo Li, Songyang Zhang, Wangbo Zhao, Yike Yuan, Jiaqi Wang, Conghui He, Ziwei Liu, and 1 others. 2024a. Mmbench: Is your multi-modal model an all-around player? In [ECCV](#), pages 216–233.

Yuliang Liu, Zhang Li, Mingxin Huang, Biao Yang, Wenwen Yu, Chunyuan Li, Xu-Cheng Yin, Cheng-Lin Liu, Lianwen Jin, and Xiang Bai. 2024b. Ocrbench: on the hidden mystery of ocr in large multimodal models. [Science China Information Sciences](#), 67(12):220102.

Zechun Liu, Changsheng Zhao, Igor Fedorov, Bilge Soran, Dhruv Choudhary, Raghuraman Krishnamoorthi, Vikas Chandra, Yuandong Tian, and Tijmen Blankevoort. 2024c. Spinquant: Llm quantization with learned rotations. [arXiv preprint arXiv:2405.16406](#).

Yuxiao Ma, Huixia Li, Xiawu Zheng, Feng Ling, Xuefeng Xiao, Rui Wang, Shilei Wen, Fei Chao, and Rongrong Ji. 2024. Affinequant: Affine transformation quantization for large language models. [arXiv preprint arXiv:2403.12544](#).

Peter Markstein. 2008. The new ieee-754 standard for floating point arithmetic.

Ahmed Masry, Xuan Long Do, Jia Qing Tan, Shafiq Joty, and Enamul Hoque. 2022. Chartqa: A benchmark for question answering about charts with visual and logical reasoning. In [Findings of ACL](#), pages 2263–2279.

Stephen Merity, Caiming Xiong, James Bradbury, and Richard Socher. 2016. Pointer sentinel mixture models. [arXiv preprint arXiv:1609.07843](#).

Asit Mishra, Dusan Stosic, Simon Layton, and Paulius Micikevicius. 2025. Recipes for pre-training llms with mxfp8. [arXiv preprint arXiv:2506.08027](#).

Markus Nagel, Marios Fournarakis, Rana Ali Amjad, Yelysei Bondarenko, Mart Van Baalen, and Tijmen Blankevoort. 2021. A white paper on neural network quantization. [arXiv preprint arXiv:2106.08295](#).

openPangu Team. 2025a. [openpangu-embedded-7b-v1.1](#).

Huawei openPangu Team. 2025b. [openpangu-vl-7b: A multi-model large language model designed and optimized for ascend npus](#).

Bita Darvish Rouhani, Ritchie Zhao, Ankit More, Mathew Hall, Alireza Khodamoradi, Summer Deng, Dhruv Choudhary, Marius Cornea, Eric Dellingler, Kristof Denolf, and 1 others. 2023. Microscaling data formats for deep learning. [arXiv preprint arXiv:2310.10537](#).

Keisuke Sakaguchi, Ronan Le Bras, Chandra Bhagavatula, and Yejin Choi. 2021. Winogrande: An adversarial winograd schema challenge at scale. [Communications of the ACM](#), 64(9):99–106.

Wenqi Shao, Mengzhao Chen, Zhaoyang Zhang, Peng Xu, Lirui Zhao, Zhiqian Li, Kaipeng Zhang, Peng Gao, Yu Qiao, and Ping Luo. 2023. Omniquant: Omnidirectionally calibrated quantization for large language models. [arXiv preprint arXiv:2308.13137](#).

Yuantian Shao, Peisong Wang, Yuanteng Chen, Chang Xu, Zhihui Wei, and Jian Cheng. 2025. Block rotation is all you need for mxfp4 quantization. [arXiv preprint arXiv:2511.04214](#).

Amanpreet Singh, Vivek Natarjan, Meet Shah, Yu Jiang, Xinlei Chen, Dhruv Batra, Devi Parikh, and Marcus Rohrbach. 2019. Towards vqa models that can read. In [CVPR](#), pages 8317–8326.

Yuxuan Sun, Ruikang Liu, Haoli Bai, Han Bao, Kang Zhao, Yuening Li, Jiaxin Hu, Xianzhi Yu, Lu Hou, Chun Yuan, and 1 others. 2024. Flatquant: Flatness matters for llm quantization. [arXiv preprint arXiv:2410.09426](#).

Yehui Tang, Yichun Yin, Yaoyuan Wang, Hang Zhou, Yu Pan, Wei Guo, Ziyang Zhang, Miao Rang, Fangcheng Liu, Naifu Zhang, and 1 others. 2025. Pangu ultra moe: How to train your big moe on ascend npus. [arXiv preprint arXiv:2505.04519](#).

Ajay Tirumala and Raymond Wong. 2024. Nvidia blackwell platform: Advancing generative ai and accelerated computing. In [HCS](#), pages 1–33.

Albert Tseng, Tao Yu, and Youngsuk Park. 2025. Training LLMs with MXFP4. In [AISTATS](#).

Hongyu Wang, Shuming Ma, Li Dong, Shaohan Huang, Huaijie Wang, Lingxiao Ma, Fan Yang, Ruiping Wang, Yi Wu, and Furu Wei. 2023. Bitnet: Scaling 1-bit transformers for large language models. [arXiv preprint arXiv:2310.11453](#).

Peng Wang, Shuai Bai, Sinan Tan, Shijie Wang, Zhihao Fan, Jinze Bai, Keqin Chen, Xuejing Liu, Jialin Wang, Wenbin Ge, Yang Fan, Kai Dang, Mengfei Du, Xuancheng Ren, Rui Men, Dayiheng Liu, Chang Zhou, Jingren Zhou, and Junyang Lin. 2024. Qwen2-vl: Enhancing vision-language model’s perception of the world at any resolution. [arXiv preprint arXiv:2409.12191](#).

Guangxuan Xiao, Ji Lin, Mickael Seznec, Hao Wu, Julien Demouth, and Song Han. 2023. Smoothquant: Accurate and efficient post-training quantization for large language models. In [ICML](#), pages 38087–38099.

Yufei Xue, Yushi Huang, Jiawei Shao, and Jun Zhang. 2025. Vlmq: Efficient post-training quantization for large vision-language models via hessian augmentation. [arXiv preprint arXiv:2508.03351](#).

JiangYong Yu, Sifan Zhou, Dawei Yang, Shuo Wang, Shuoyu Li, Xing Hu, Chen Xu, Zukang Xu, Changyong Shu, and Zhihang Yuan. 2025. Mquant: Unleashing the inference potential of multimodal large language models via full static quantization. [arXiv preprint arXiv:2502.00425](#).

Zhihang Yuan, Yuzhang Shang, Yang Zhou, Zhen Dong, Zhe Zhou, Chenhao Xue, Bingzhe Wu, Zhikai Li, Qingyi Gu, Yong Jae Lee, and 1 others. 2024. Llm inference unveiled: Survey and roofline model insights. [arXiv preprint arXiv:2402.16363](#).

Xiang Yue, Yuansheng Ni, Kai Zhang, Tianyu Zheng, Ruoqi Liu, Ge Zhang, Samuel Stevens, Dongfu Jiang, Weiming Ren, Yuxuan Sun, and 1 others. 2024. Mmmu: A massive multi-discipline multimodal understanding and reasoning benchmark for expert agi. In [CVPR](#), pages 9556–9567.

Rowan Zellers, Ari Holtzman, Yonatan Bisk, Ali Farhadi, and Yejin Choi. 2019. Hellaswag: Can a machine really finish your sentence? [arXiv preprint arXiv:1905.07830](#).

Kaichen Zhang, Bo Li, Peiyuan Zhang, Fanyi Pu, Joshua Adrian Cahyono, Kairui Hu, Shuai Liu, Yuanhan Zhang, Jingkang Yang, Chunyuan Li, and 1 others. 2025. Lmms-eval: Reality check on the evaluation of large multimodal models. In [Findings of NAACL](#), pages 881–916.

A Appendix

A.1 Benchmarks and Evaluation Details

Below, we briefly introduce the benchmarks and the evaluation details in this study.

Non-Reasoning Benchmarks. **PIQA**: It is a physical commonsense reasoning and corresponding benchmark dataset, which was designed to investigate the physical knowledge of existing models. **Winogrande**: Winogrande is a collection of 44k problems formulated as a fill-in-a-blank task with binary options, and the goal is to choose the right option for a given sentence, which requires commonsense reasoning. **Hellaswag**: It is a commonsense inference benchmark designed to challenge language models with adversarially filtered multiple-choice questions. **ARC-Easy & ARC-Challenge**: The ARC dataset consists of 7,787 science exam questions drawn from a variety of sources. Each question has a multiple-choice structure (typically 4 answer options). ARC-Easy contains 5,197 easy questions, and ARC-Challenge contains 2,590 hard questions. For all non-reasoning benchmarks, we use lm-evaluation-harness (Gao et al., 2024) with the vllm (Kwon et al., 2023) backend for evaluation.

Reasoning Benchmarks. **MATH500**: A benchmark that contains a mix of easy and hard mathematical problems designed to test comprehensive reasoning abilities. We evaluate model performance using **Avg@1** (*i.e.*, the accuracy of the first generated answer). **AIME24**: It contains 30 problems from the American Invitational Mathematics Examination (AIME) 2024. **AIME25**: It contains 30 problems from the American Invitational Mathematics Examination (AIME) 2025. Following standard practice for high-stakes math benchmarks, we report results using **Avg@16** for AIME24 and AIME25, which averages accuracy over 16 independently sampled reasoning traces per problem. For all reasoning benchmarks, we follow (openPangu Team, 2025a) to evaluate openPangu-Embedded-7B-V1.1 without extra CoT prompts across all reasoning benchmarks. We use Lighteval (Habib et al., 2023) with the vllm (Kwon et al., 2023) backend for evaluation with a sampling temperature of 1.0 and top-p of 0.8. The maximum sequence length of the model is limited to 131,072.

Image-Text Benchmarks. **OCR-Bench**: OCR-Bench is a comprehensive evaluation bench-

mark designed to assess the OCR capabilities of Large Multimodal Models, which contains 1000 question-answer pairs, including Text Recognition, SceneText-Centric VQA, Document-Oriented VQA, Key Information Extraction, and Handwritten Mathematical Expression Recognition. **MM-Bench**: It is a collection of benchmarks to evaluate the multimodal understanding capability of large vision language models (LVLMs). **TextVQA**: TextVQA evaluates a model’s ability to read and reason about text present in images. We use the validation set, which contains 5,000 question-answer pairs. **ChartQA**: A benchmark focused on chart understanding and reasoning. **MME**: A benchmark that evaluates LVLMs across multiple dimensions, including perception, cognition, and object hallucination. **MMIU**: This is a challenging multidisciplinary problem involving benchmarking across fields such as art, engineering, law, and medicine. For all Image-Text benchmarks, we use metrics in LMMs-Eval (Zhang et al., 2025) with the vllm (Kwon et al., 2023) backend for evaluation. In the main tables, Vision Transformer (ViT) is quantized by RTN, and LLM is quantized by different PTQ methods.

A.2 Additional Experiments

A.2.1 Results on Reasoning Benchmarks

We provide the detailed results on reasoning benchmarks in Table 7.

A.2.2 Results on openPangu-VL-7B

We provide the detailed evaluation results on openPangu-VL-7B for reference (see Table 8).

A.2.3 Results under More Quantization Scenarios

Below, we report the results of openPangu-Embedded-7B-V1.1 and Llama-3.1-8B-Instruct under more bit-width configurations (including W4A16 and W4A8KV8) as shown in Table 9 and Table 10, respectively.

Results on W4A16. According to Table 9 and Table 10, even though activations remain at high precision (16-bit), quantizing weights to 4 bits already leads to a noticeable performance drop for most methods. For instance, QuaRot achieves only a 95.27% recovery rate on openPangu-Embedded-7B-V1.1, falling into the **risky** regime (<97%). Interestingly, when comparing W4A16 with the more aggressive W4A8 setting, we observe that the primary bottleneck lies in 4-bit weight quantization

Bits	Method	ACC (0-shot) \uparrow			Avg.	Recovery (%)
		AIME24	AIME25	MATH-500		
BF16	–	77.29	71.25	96.20	81.58	100.00
W8A8	RTN	78.33	67.71	94.80	80.28	98.41
	SpinQuant*	76.88	68.96	96.20	80.68	99.00
	FlatQuant*	74.58	65.62	94.20	78.13	95.78
	SmoothQuant*	77.29	67.71	95.40	80.13	98.23
	GPTQ	80.00	68.54	95.00	81.18	99.51
W4A8	RTN	70.00	61.46	94.80	75.42	92.45
	SpinQuant*	73.96	66.46	94.00	78.14	95.78
	FlatQuant*	71.67	65.62	95.40	77.56	95.08
	SmoothQuant*	73.96	62.29	95.60	77.28	94.73
	GPTQ	72.50	66.04	94.80	77.78	95.34
W4A4	RTN	62.50	54.37	94.20	70.36	86.24
	SpinQuant*	47.26	44.37	90.80	60.81	74.54
	FlatQuant*	68.75	57.92	93.60	73.42	90.00
	SmoothQuant*	61.25	54.58	93.00	69.61	85.33
	GPTQ	66.67	55.21	93.00	71.63	87.80

Table 7: Comprehensive comparison of PTQ methods on **openPangu-Embedded-7B-V1.1** under W8A8, W4A8, and W4A4 in terms of **reasoning** downstream task accuracy. * denotes the variant integrated with the GPTQ algorithm. Recovery (%) is computed relative to the BF16 baseline.

itself, rather than 8-bit activation compression, as the performance of most methods only slightly decreases. For example, on openPangu-Embedded-7B-V1.1, SpinQuant’s recovery rate drops only slightly from 95.10% (W4A16) to 94.46% (W4A8), while FlatQuant’s recovery rate even improves from 96.87% (W4A16) to 97.12% (W4A8). These findings suggest that even the 4-bit weight quantization alone constitutes a significant challenge.

Results on W4A8KV8. We further investigated the impact of 8-bit KV cache quantization. According to Table 9 and Table 10, comparing the W4A8 setting with W4A8KV8, some methods maintain stable performance when the KV cache is 8-bit quantized. For example, on openPangu-Embedded-7B-V1.1, RTN, SpinQuant, and FlatQuant show only minor changes in accuracy recovery rate, changing from 95.44%, 94.46%, and 97.12% to 95.14%, 94.33%, and 97.42%, respectively. However, other methods exhibit noticeable degradation. For instance, the accuracy recovery rate of SmoothQuant and GPTQ drops from 96.33% and 97.03% to 94.96% and 95.32%, respectively. These results indicate that 8-bit KV cache quantization is not risk-free, and different quantization methods exhibit varying degrees of robustness to KV cache

precision reduction.

A.3 Visualization of Activations

Figure 5 shows the activation distributions of the `q_proj` module in Layer 8 of openPangu-Embedded-7B-V1.1 under various quantization methods.

A.4 Use of AI Assistants

We acknowledge that we used AI to help improve the manuscript, mainly for grammar, phrasing, and overall clarity. AI was also briefly used to fix small errors and syntax in the code included in the work.

Bits	Method	OCR Bench	MMBench	MMBench ^{CN}	TextVQA	ChartQA	MME	MMMU	Recovery (%)
BF16	-	918	85.46	85.4	83.92	87.68	2287	54.5	100.00
W8A8	RTN	906	85.05	85.71	83.78	88.04	2329	51.8	99.39
	QuaRot	899	85.54	84.54	83.64	87.32	2263	53.9	99.16
	QuaRot*	898	85.80	84.36	83.48	87.52	2266	52.4	98.79
	SpinQuant	905	85.42	85.31	83.84	87.25	2285	54.2	99.60
	SpinQuant*	904	85.46	85.21	83.71	87.24	2285	54.3	99.58
	FlatQuant	908	85.20	85.05	83.79	87.42	2280	54.3	99.58
	FlatQuant*	908	85.46	85.65	84.14	87.56	2285	54.6	99.92
	AWQ	911	85.22	85.20	83.76	87.68	2290	54.0	99.68
	SmoothQuant	914	85.29	85.48	82.71	87.66	2289	54.4	99.70
W4A8	SmoothQuant*	908	85.29	85.21	83.14	87.25	2280	54.5	99.54
	GPTQ	908	85.71	85.22	83.93	87.72	2295	54.3	99.86
	RTN	887	83.08	82.90	82.47	86.52	2237	51.3	97.11
	QuaRot	872	81.97	80.41	82.16	86.12	2270	47.7	95.42
	QuaRot*	884	84.86	81.79	82.90	86.88	2269	50.7	97.35
W4A8	SpinQuant	894	83.08	81.70	82.94	87.32	2231	49.6	96.75
	SpinQuant*	911	84.10	83.08	83.65	86.80	2291	53.3	98.80
	FlatQuant	906	84.18	83.42	83.44	87.52	2280	53.3	98.80
	FlatQuant*	905	84.27	84.54	83.49	87.80	2259	53.3	98.91
	AWQ	884	83.59	82.65	82.80	86.48	2264	53.2	97.82
	SmoothQuant	884	83.16	82.39	82.71	87.16	2259	52.7	97.65
	SmoothQuant*	903	83.93	84.11	83.23	87.48	2289	51.3	98.32
	GPTQ	898	85.63	84.19	83.11	87.24	2267	52.8	98.73
	RTN	878	81.55	80.50	80.77	85.88	2193	52.3	95.91
W4A4	QuaRot	823	68.11	53.61	76.26	68.10	2005	40.1	80.27
	QuaRot*	844	74.40	62.63	77.97	78.84	2034	44.5	86.54
	SpinQuant	852	72.45	63.06	78.56	83.40	1988	41.3	86.12
	SpinQuant*	874	77.98	75.09	80.45	85.90	2198	48.3	93.28
	FlatQuant	866	82.99	81.96	81.43	86.44	2191	50.0	95.80
	FlatQuant*	896	84.01	81.7	83.15	86.96	2196	50.3	96.88
	AWQ	880	81.80	80.67	81.04	85.80	2226	50.5	95.78
	SmoothQuant	867	80.61	78.69	80.89	85.64	2215	52.4	95.42
	SmoothQuant*	892	81.63	80.15	82.2	87.04	2246	50.6	96.40
	GPTQ	879	82.56	80.58	81.00	85.88	2277	51.0	96.33

Table 8: Comparison of PTQ methods on **openPangu-VL-7B** under W8A8, W4A8, and W4A4 quantization across multimodal benchmarks. * denotes the variant integrated with the GPTQ algorithm.

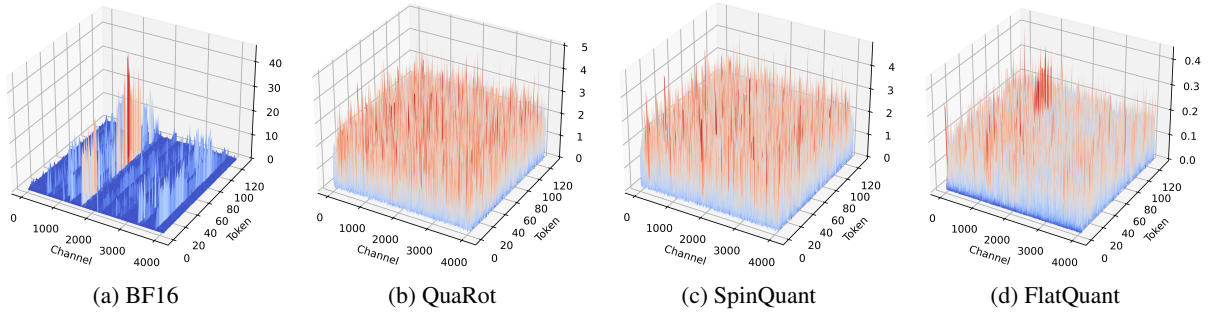


Figure 5: Activation distributions of the q_proj module in layer 8 of openPangu-Embedded-7B-V1.1 with different quantization methods. Each subplot shows the activations observed during inference, highlighting how quantization methods alter the dynamic range and distribution.

Bits	Method	ACC (0-shot) \uparrow							PPL \downarrow
		ARC-C	ARC-E	HellaSwag	PIQA	Winogrande	Avg.	Recovery. (%)	
BF16	-	42.75	67.26	62.86	73.50	60.62	61.40	100.00	34.89
W8A8	RTN	44.03	66.25	61.74	73.61	57.77	60.68	98.83	35.75
	QuaRot	42.24	65.95	62.45	72.42	60.69	60.75	98.94	35.21
	QuaRot*	42.83	68.22	62.18	73.78	60.96	61.59	100.32	35.75
	SpinQuant	42.49	67.34	62.42	72.31	60.30	60.97	99.31	35.49
	SpinQuant*	42.58	68.43	62.52	73.94	59.59	61.41	100.02	33.04
	FlatQuant	43.43	68.64	62.25	73.78	59.04	61.43	100.05	30.96
	FlatQuant*	43.86	69.23	62.33	74.05	61.33	62.16	101.24	30.87
	AWQ	41.98	68.48	61.16	72.58	61.09	61.06	99.45	38.00
	SmoothQuant	42.58	66.50	62.08	72.69	59.19	60.61	98.71	35.25
	SmoothQuant*	42.15	66.67	61.84	72.36	59.59	60.52	98.57	35.00
W4A16	MR-GPTQ	43.09	67.80	62.84	73.72	59.91	61.47	100.12	34.57
	GPTQ	42.92	67.13	61.66	72.69	57.85	60.45	98.46	34.75
	RTN	41.72	66.04	59.06	72.36	58.64	59.56	97.01	39.99
	QuaRot	40.53	63.05	58.25	71.76	57.70	58.26	94.89	43.29
	QuaRot*	40.27	64.35	58.65	71.44	57.62	58.47	95.22	40.50
	SpinQuant	39.25	63.13	58.35	72.09	59.12	58.39	95.10	38.11
	SpinQuant*	41.55	68.18	61.02	72.85	60.38	60.80	99.02	35.26
	FlatQuant	39.68	65.45	60.50	72.80	58.96	59.48	96.87	37.68
	FlatQuant*	41.81	66.92	60.72	72.42	59.12	60.20	98.05	37.62
	AWQ	41.81	66.33	58.37	73.67	58.80	59.80	97.39	40.00
W4A8	SmoothQuant	40.44	66.08	59.71	72.80	57.22	59.25	96.50	43.25
	SmoothQuant*	42.49	66.75	60.46	73.56	58.80	60.41	98.39	38.75
	MR-GPTQ	-	-	-	-	-	-	-	-
	GPTQ	40.80	65.50	60.80	72.20	59.75	59.81	97.41	37.00
	RTN	39.59	65.24	58.70	71.60	57.85	58.60	95.44	42.17
	QuaRot	40.10	64.10	57.95	72.69	57.70	58.51	95.29	40.87
	QuaRot*	40.02	65.07	58.54	71.44	57.62	58.54	95.84	43.83
	SpinQuant	39.59	61.57	58.56	72.09	58.17	58.00	94.46	38.94
	SpinQuant*	42.41	67.85	60.74	72.91	58.8	60.54	98.60	34.75
	FlatQuant	40.78	66.54	60.15	72.52	58.17	59.63	97.12	37.67
W4A8KV8	FlatQuant*	42.15	67.63	60.54	72.80	57.38	60.10	97.89	37.72
	AWQ	39.85	66.25	58.13	73.07	58.17	59.09	96.25	41.75
	SmoothQuant	40.78	66.20	58.82	72.47	57.46	59.15	96.33	43.25
	SmoothQuant*	41.64	67.47	59.88	73.07	58.88	60.19	98.03	40.00
	MR-GPTQ	40.87	66.84	60.64	72.63	57.93	59.78	97.36	39.19
	GPTQ	40.96	65.51	59.48	72.42	59.51	59.58	97.03	37.50
	RTN	40.19	63.34	57.94	72.03	58.56	58.41	95.14	44.16
	QuaRot	39.93	63.76	57.73	72.03	57.93	58.28	94.92	41.74
	QuaRot*	39.93	64.69	58.13	71.06	59.27	58.62	95.47	42.50
	SpinQuant	37.63	62.96	58.06	72.14	58.80	57.92	94.33	39.81
W4A4	SpinQuant*	43.17	65.78	60.34	72.36	60.69	60.47	98.48	36.56
	FlatQuant	40.61	68.10	59.58	72.31	58.48	59.82	97.42	38.66
	FlatQuant*	41.81	66.29	60.05	71.76	58.01	59.58	97.03	39.28
	AWQ	39.16	64.94	56.87	72.31	58.17	58.29	94.94	44.50
	SmoothQuant	39.85	64.60	58.20	71.87	56.99	58.30	94.96	45.25
	SmoothQuant*	42.49	64.44	59.15	71.76	58.96	59.36	96.68	41.25
	MR-GPTQ	-	-	-	-	-	-	-	-
	GPTQ	39.51	63.41	58.89	71.00	59.83	58.53	95.32	39.25
	RTN	38.48	61.53	56.42	70.46	56.91	56.76	92.45	49.33
	QuaRot	36.43	56.19	51.24	66.76	54.54	53.03	86.37	56.19
W4A4	QuaRot*	36.09	59.30	53.06	68.55	55.33	54.47	88.71	53.75
	SpinQuant	34.64	57.24	52.82	68.39	55.49	53.72	87.49	51.09
	SpinQuant*	37.88	60.4	55.34	69.53	57.22	56.07	91.33	46.28
	FlatQuant	39.93	65.82	57.07	71.00	56.04	57.97	94.42	38.36
	FlatQuant*	40.19	66.84	58.13	69.80	57.54	58.50	95.28	36.40
	AWQ	37.08	63.76	54.49	71.06	57.70	56.82	92.54	46.00
	SmoothQuant	38.99	65.07	55.81	70.80	56.70	57.47	93.60	52.00
	SmoothQuant*	38.65	64.60	56.74	70.73	57.62	57.67	93.92	43.57
	MR-GPTQ	38.99	63.43	57.19	69.48	58.96	57.61	93.83	42.17
	GPTQ	39.25	62.75	57.47	69.91	56.99	57.27	93.28	44.50

Table 9: Comprehensive comparison of PTQ methods on **openPangu- Embedded-7B-V1.1** under W8A8, W4A8, and W4A4 in terms of **non-reasoning** downstream task accuracy and perplexity. * denotes the variant integrated with the GPTQ algorithm.

Bits	Method	ACC (0-shot) \uparrow							PPL \downarrow
		ARC-C	ARC-E	HellaSwag	PIQA	Winogrande	Avg.	Recovery (%)	
BF16	–	55.20	79.63	79.15	81.07	73.95	73.80	100.00	–
W8A8	RTN	53.50	78.45	79.11	80.14	73.64	72.97	98.87	7.31
	QuaRot	55.72	80.09	78.76	80.58	73.64	73.76	99.94	7.39
	QuaRot*	56.4	80.81	78.84	81.01	74.35	74.28	100.65	7.40
	SpinQuant	55.89	80.18	78.60	80.79	74.51	73.99	100.26	7.39
	SpinQuant*	54.35	80.09	78.12	80.2	73.8	73.31	99.34	7.41
	FlatQuant	55.80	79.46	78.99	81.12	73.80	73.83	100.05	7.27
	FlatQuant*	54.69	79.42	78.56	80.63	74.19	73.50	99.59	7.33
	AWQ	54.27	79.17	78.48	80.74	73.80	73.29	99.31	7.34
	SmoothQuant	55.38	79.08	79.14	81.23	74.51	73.87	100.09	7.34
	SmoothQuant*	55.03	79.63	78.73	81.39	73.88	73.73	99.91	7.34
W4A16	MR-GPTQ	55.38	79.12	78.99	81.01	73.95	73.69	99.85	7.24
	GPTQ	54.69	79.12	78.47	80.79	74.35	73.48	99.57	7.33
	RTN	53.24	77.90	77.32	80.36	73.80	72.52	98.27	7.64
	QuaRot	48.98	75.67	76.68	78.56	70.64	70.11	94.99	8.28
	QuaRot*	53.33	77.65	77.00	79.43	73.40	72.16	97.78	7.75
	SpinQuant	50.43	75.13	76.17	78.67	71.51	70.38	95.37	8.38
	SpinQuant*	52.47	78.37	77.35	80.2	73.4	72.36	98.05	7.70
	FlatQuant	53.92	77.36	77.58	80.25	73.32	72.49	98.22	7.86
	FlatQuant*	–	–	–	–	–	–	–	–
	AWQ	53.92	79.46	77.73	80.25	73.40	72.95	98.85	7.62
W4A8	SmoothQuant	53.50	78.48	77.85	80.25	74.51	72.92	98.80	7.62
	SmoothQuant*	53.16	76.81	77.61	79.11	73.01	71.94	97.48	7.75
	MR-GPTQ	–	–	–	–	–	–	–	–
	GPTQ	53.92	79.04	77.65	80.96	73.48	73.01	98.93	7.71
	RTN	53.07	76.81	77.04	80.03	73.48	72.09	97.68	7.71
	QuaRot	49.15	75.93	76.37	78.29	71.03	70.15	95.06	8.45
	QuaRot*	52.65	79.67	77.86	80.52	73.40	72.82	98.67	7.95
	SpinQuant	49.91	75.59	76.10	78.07	71.90	70.31	95.28	8.50
	SpinQuant*	52.82	78.37	76.96	79.6	73.32	72.21	97.85	7.84
	FlatQuant	53.84	80.26	77.27	80.03	71.82	72.64	98.43	7.87
W4A8KV8	FlatQuant*	53.84	80.26	77.27	80.03	71.82	72.64	97.95	7.81
	AWQ	53.84	79.25	77.55	79.98	73.88	72.90	98.78	7.75
	SmoothQuant	54.01	77.61	77.77	79.98	74.98	72.87	98.74	7.75
	SmoothQuant*	52.96	77.02	77.42	78.63	70.64	71.33	96.67	8.70
	MR-GPTQ	54.52	78.62	77.28	80.47	73.80	72.94	98.83	7.83
	GPTQ	53.5	79.59	79.71	81.18	73.6	73.52	99.62	7.87
	RTN	52.22	77.02	76.91	79.92	73.64	71.94	97.48	7.31
	QuaRot	50.09	76.09	76.25	78.78	70.32	70.31	95.27	8.46
	QuaRot*	52.73	79.92	77.78	80.03	73.40	72.77	98.61	7.97
	SpinQuant	50.09	75.25	75.89	77.91	71.43	70.31	95.28	8.50
W4A4	SpinQuant*	52.9	78.32	77.44	80.58	72.61	72.37	98.06	7.79
	FlatQuant	54.86	79.55	77.39	78.94	71.98	72.54	98.30	7.87
	FlatQuant*	53.84	78.83	77.70	79.71	73.09	72.63	98.42	7.72
	AWQ	54.52	79.12	77.53	79.87	72.93	72.79	98.64	7.75
	SmoothQuant	53.33	77.48	77.57	80.30	74.98	72.73	98.55	7.73
	SmoothQuant*	51.54	79.17	77.54	79.11	72.77	72.03	97.60	7.87
	MR-GPTQ	–	–	–	–	–	–	–	–
	GPTQ	54.15	78.62	77.37	80.09	73.35	72.72	98.53	7.34
	RTN	49.66	75.80	75.48	79.05	70.48	70.09	94.98	8.27
	QuaRot	44.11	71.63	71.82	75.14	64.88	65.52	88.78	10.34
W4A4	QuaRot*	49.15	74.62	74.26	77.48	68.98	68.90	93.36	9.12
	SpinQuant	43.09	67.26	70.71	74.92	65.98	64.39	87.25	10.40
	SpinQuant*	49.15	74.54	74.38	76.99	69.53	68.92	93.38	9.01
	FlatQuant	52.05	77.27	76.89	79.49	70.64	71.27	96.57	8.03
	FlatQuant*	51.19	78.58	76.77	78.94	71.67	71.43	96.79	8.06
	AWQ	52.30	77.95	76.13	78.92	69.46	70.95	96.14	8.25
	SmoothQuant	51.37	76.52	76.12	79.00	72.38	71.08	96.31	8.25
	SmoothQuant*	50.51	73.36	75.27	76.82	67.17	68.63	92.98	8.50
	MR-GPTQ	50.85	75.46	76.02	79.82	70.80	70.59	95.65	8.34
	GPTQ	50.68	77.65	75.66	78.18	70.24	70.48	95.50	8.37

Table 10: Comprehensive comparison of PTQ methods on **Llama-3.1-8B-Instruct** under W8A8, W4A8, and W4A4 in terms of **non-reasoning** downstream task accuracy and perplexity. * denotes the variant integrated with the GPTQ algorithm.